Available online at www.easdprocedia.org
EASD Procedia EURODYN (2020) 2985-3004

EASD Procedia

EURODYN 2020
XI International Conference on Structural Dynamics
M. Papadrakakis, M. Fragiadakis, C. Papadimitriou (eds.)
Athens, Greece, 23–26 November 2020

TIME DOMAIN BEM-FEM COUPLING FOR SEISMIC SOIL-STRUCTURE INTERACTION ANALYSES CONCEIVED FOR AN ANSYS-MATLAB WORKFLOW

Francesca Taddei[1], **Bettina Chocholaty**[2], **and Gerhard Müller**[1]

[1]Chair of Structural Mechanics TUM Department of Civil, Geo and Environmental Engineering
Arcisstr. 21, 80333, Munich
e-mail: {francesca.taddei, gerhard.mueller}@tum.de

[2] Chair of Vibro-Acoustics of Vehicles and Machines TUM Department of Mechanical Engineering
Boltzmannstr. 15, 85748 Garching near Munich
e-mail: bettina.chocholaty@tum.de

Keywords: Soil-Structure Interaction, Boundary Element Method, Finite Element Method, BEM-FEM coupling, Time Domain.

Abstract. *In this contribution, we present the implementation of the coupling between the Finite Element Method (FEM) and the Boundary Element Method (BEM) in the time domain, for the analysis of the Soil-Structure Interaction (SSI) in the three dimensional space. The Boundary Element Method is based on the transient fundamental solutions for the half-space. The coupling between the BEM and the FEM is obtained using the soil's stiffness matrix and the soil reaction forces, which result from a convolution integral. The coupling is implemented linking the software MATLAB with the software ANSYS. The system of equations is solved in ANSYS and within the solution step MATLAB is activated to calculate the soil's stiffness matrix and the interaction forces at the interface between soil and structures at the current time step. Verification examples for static and dynamic cases are presented. A case study for a seismic excitation is presented to show the applicability of the proposed method.*

ISSN:2311-9020
Peer-review under responsibility of the Organizing Committee of EURODYN 2020.
doi: 10.47964/1120.9244.20361

1 INTRODUCTION

The dynamic interplay between the buildings and the underlying soil is referred to as Soil-Structure Interaction (SSI). The soil acts both as a compliant support with a frequency-dependent flexibility and as a energy absorber, due to its infinite size. For certain combinations of buildings and soil, the SSI may lead to an amplification of the dynamic response w.r.t. the static response of the whole system, to a shift of the natural frequencies of the buildings and to a change in damping properties. Therefore, it is important to account for the dynamic behavior of the soil and its effect on the dynamic behaviour of the structures placed on it.. The main difficulty of simulating the SSI is related to the infinite size of the soil, for which the Sommerfeld radiation condition must be fulfilled.

Different methods exist to account for the SSI in seismic analysis of buildings, the most popular of which are the Finite Element Method (FEM), the Finite Difference Method (FDM) and the Boundary Element Method (BEM). A detailed state of the art can be found in [1].

For FEM the whole domain is discretised whereas in the BEM only the boundaries are divided into elements. Consequently, the dimension of the problem is reduced by one when using BEM. This leads to less necessary storage space. Moreover, the BEM can achieve higher accuracy for the results, since it uses fundamental solutions as weighting functions. These fundamental solutions fulfill exactly the boundary conditions.

Although research has been conducted on boundary elements since the 1960s, BEM is not as established as the FEM, mainly due to the fully populated system of equations generated by the BEM and the requirement of the existence of suitable fundamental solutions for the investigate soil systems (such as an homogeneous half space, a layered half space, etc...). Additionally, several commercial tools made the FEM user-friendly and versatile, while the BEM is rarely available as a ready-to-use black box. An extensive overview of the development of BEM can be found in [2].

The BEM for SSI can be used both in the Time Domain (TD) and in the Frequency Domain (FD), depending on the available fundamental solutions (also called Green's functions). The TD-BEM can be used for nonlinear problems and can lead to less computational effort for transient loads with a narrow frequencies spectrum. As a matter of fact, the transient fundamental solutions have a bounded support, while the FD fundamental solutions never vanish.

From general descriptions of the coupling of BEM and FEM for elastodynamics [3][4][5], the application to SSI problems was straightforward [6].

Further improvements of the BEM for SSI were achieved by using fundamental solutions for the half-space instead of the full space [7]. Depending on the given problem, the suitable fundamental solution can be chosen among the available ones [8] to optimize the computation. Several studies have been conducted on the topic of BEM for 2D- and 3D-structures in the time domain dealing with different issues, such as the choice of the suitable fundamental solutions (e.g. [9] and [10]) or the coupling of incompatible interfaces of BEM and FEM for 2D boundary elements ([11]).

Recently, Vasilev et al. [12] developed a hybrid computational tool, based on the FEM/BEM coupling. The hybrid numerical scheme is realized via the sub-structure approach, integrating the seismically active far-field geological media as a macro-finite element in the commercial program ANSYS. Here, they assume a plane strain state.

Galvin and Romero [13] developed a numerical tool *SSIFiBo* in MATLAB to study dynamic soil-structure interaction problems. The model is based on a three dimensional TD-BEM. This model allows computing structural forced-vibrations, as well as seismic responses.

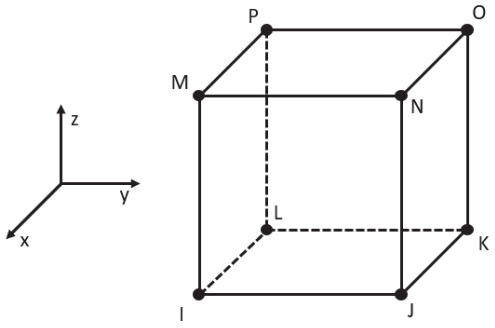

Figure 1: Notation of nodes for *SOLID185*, according to [18, p. 960]

Schepers [14] improved an existing customization of ANSYS [15] [16] [17] which allows FEM-BEM coupling of structures at the surface of an arbitrarily layered half-space, both in time and frequency domain.

In this work, we present the *Ssibefe* tool, a FEM-BEM coupling where the FEM subsystem (the building) is modeled using ANSYS and the BEM subsystem (the soil) is treated using MATLAB. The loading can be applied to the FEM elements and nodes and/or can be defined as a propagating transient plane wave in the soil with an arbitrary angle of incidence w.r.t the surface. Pre- and postprocessing is performed in ANSYS. The TD fundamental solutions for the homogenous half-space are taken from [8] and the procedure for the implementation is similar to the one described by [15], [16] and [17].

2 METHODS

2.1 MODELLING THE STRUCTURE WITH THE FINITE ELEMENT METHOD

The equation of motion for the structure reads:

$$\mathbf{M}\ddot{\mathbf{u}}(t) + \mathbf{C}\dot{\mathbf{u}}(t) + \mathbf{K}\mathbf{u}(t) = \mathbf{P}(t) + \mathbf{Q}(t), \tag{1}$$

where $\mathbf{M}$ is the mass matrix, $\mathbf{C}$ the damping matrix, $\mathbf{K}$ the stiffness matrix, $\mathbf{u}(t)$ the displacements and $\mathbf{P}(t)$ the external loading. All the aforementioned vectors and matrices can be determined as usual by means of classical FEM formulations. The key vector in this formulation is the vector $\mathbf{Q}(t)$, which contains the soil reactions at the interaction nodes. This is unknown and represents the influence of the soil as nodal forces, which result from the contact pressure at the soil–structure interface. This can be computed with the BEM formulation, described in section 2.2.

The analysis of the finite system is done with the commercial software *Ansys Mechanical APDL 2019 R2*. The structure is modelled by 3D solid elements, specifically the *SOLID185*-elements, which consist of 8 nodes [18]. The arrangement of the nodes is depicted in fig. 1.

2.2 MODELLING THE SOIL WITH THE BOUNDARY ELEMENT METHOD

2.2.1 Theoratical Background

At the heart of the TD-BEM used here lies the transient fundamental solutions for the 3D the half space subjected to a vertical or horizontal unit point load on the surface, that changes

in time as a Heaviside function (s. annex A). These satisfy the traction-free condition at the surfaces of the soil and the Sommerfeld radiation condition.

We start from the discretized form of the boundary integral formulation of the Lamé-Navier equation [19], in absence of body forces. At first the time dependency is not considered and will be treated separately in section 2.3. The displacements $\mathbf{w}^i$ at point i on the soil surface can be written as:

$$\mathbf{c}^i\mathbf{w}^i(\mathbf{x}^i) = \sum_{e=1}^{E}\sum_{n=1}^{N} \mathbf{q}_n^e \int_{S_e} \mathbf{N}_n \mathbf{g}(\mathbf{x},\mathbf{x}^i) dS - \sum_{e=1}^{E}\sum_{n=1}^{N} \mathbf{w}_n^e \int_{S_e} \mathbf{N}_n \mathbf{t}(\mathbf{x},\mathbf{x}^i) dS \tag{2}$$

with

$\mathbf{g}(\mathbf{x},\mathbf{x}^i)$: fundamental solution for the displacements evaluated at point $\mathbf{x}^i$ for loads at $\mathbf{x}$
$\mathbf{t}(\mathbf{x},\mathbf{x}^i)$: fundamental solution for the tractions evaluated at point $\mathbf{x}^i$ for loads at $\mathbf{x}$
$\mathbf{q}_n^e$: nodal forces at point $\mathbf{x}^i$
$\mathbf{w}_n^e$: nodal displacements at point $\mathbf{x}^i$
$\mathbf{N}_n$: shape functions of nodes at point $\mathbf{x}^i$
$\mathbf{c}^i$: geometrical coefficient, which is related to the the position of the load and contains unitary values at the soil surface for a smooth boundary
N, E, S_e: number of nodes per element, number of elements and area of each element respectively.

We assume constant tractions on each boundary element. Therefore, each boundary element has only one node at the centre of the bottom surface of the coupled finite element. The elements are pictured in fig. 2a. Here, the red circled nodes define the contributing coupling nodes.

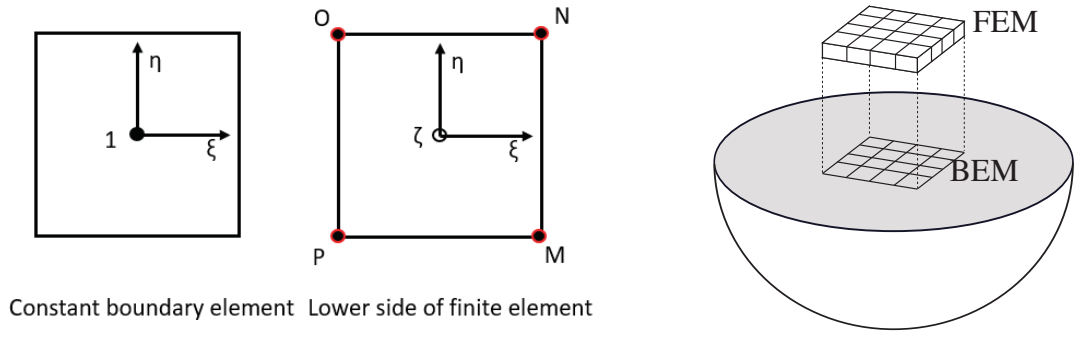

(a) Coupling nodes for constant shape functions.

(b) Coupling surface.

Figure 2: Coupling between soil and structure.

We consider Heaviside-time-varying unit forces for each nodal component of displacements and tractions. If the load position is located inside the domain, the stresses $\mathbf{t}(\mathbf{x},\mathbf{x}^i)$ on the surface are equal to zero and only the first part of the right side of eq. (2) will be considered in further derivations, leading to the following expression for the the displacements:

$$\mathbf{c}^i\mathbf{w}^i(\mathbf{x}^i) = \sum_{e=1}^{E}\sum_{n=1}^{N} \mathbf{q}_n^e \Delta\mathbf{G}_n^e \tag{3}$$

where

$$\Delta\mathbf{G}_n^e = \int_{-1}^{1}\int_{-1}^{1} \mathbf{N}_n(\xi,\eta)\mathbf{g}(\mathbf{x},\mathbf{x}^i(\xi,\eta))J(\xi,\eta)d\xi d\eta \tag{4}$$

Here, $J(\xi, \eta)$ denotes the determinant of the Jacobian for the transformation of coordinates from the original Cartesian to a local element reference coordinate system.

To obtain the flexibility matrix of the soil, the integral in eq. (3) is evaluated $(E \cdot N)^2$ times. The integral is performed for all the interaction nodes as an observation point and with the loading position being located on every interaction node (collocation point method). This leads to a matrix $\mathcal{G}^{ji}$, where the rows j indicate the loading position information whereas the columns i indicate the observation position information. Once the unitary coefficients $\mathbf{c}^i$ are included in the system matrix, eq. (3) can be written in matrix form as:

$$\mathbf{w} = \mathcal{G}\mathbf{q} \tag{5}$$

The fundamental solution $\mathbf{g}(\mathbf{x}, \mathbf{x}^i)$ is a antisymmetrical second order tensor, originally defined in cylindrical coordinates, as described in annex A:

$$\mathbf{g}^{\text{cyl}} = \begin{bmatrix} g_{rr} & 0 & g_{rz} \\ 0 & g_{\phi\phi} & 0 \\ g_{zr} & 0 & g_{zz} \end{bmatrix} \tag{6}$$

with $g_{zr} = -g_{rz}$. The transformation from cylindrical to Cartesian coordinates is performed according to [15] (s. annex B).

Following the suggestions in [20], if the loading point $\mathbf{x}$ coincides with the observation point $\mathbf{x}^i$, a $1/r$-singularity occurs. This integration is solved using a transformation to polar coordinates according to [21] (s. annex C).

Summarizing, eq. (5) says that the interaction of the soil with any other elastic body at its surface can be represented by integrals over the contact surface and a force-displacement relationship can be established to built the stiffness or flexibility matrix of the soil.

The fundamental solutions depend on the dimensionless time τ which in turn depends on on the time t. The time dependency will be treated in the next section.

2.3 Time discretization

According to [15], for the application of the proposed method in the time domain, the displacement at the current time depends on the current contact pressures and on its history and is obtained with a convolution integral. For a Heaviside loading function, the second Duhamel integral is performed:

$$\begin{aligned} \mathbf{w}(t) &= \mathcal{G}(t) \otimes \mathbf{q}(t) \\ \mathbf{w}(t) &= \mathbf{q}(0)\mathcal{G}(t) + \int_0^t \mathcal{G}(t-\tau)\frac{d\mathbf{q}(\tau)}{d\tau}d\tau = \int_0^t \mathcal{G}(t-\tau)\frac{d\mathbf{q}(\tau)}{d\tau}d\tau. \end{aligned} \tag{7}$$

The transient fundamental solutions are captured in the matrix $\mathcal{G}(t)$

$$\mathcal{G}(t) = \begin{bmatrix} \mathcal{G}_{xx}(t) & \mathcal{G}_{xy}(t) & \mathcal{G}_{xz}(t) \\ \mathcal{G}_{yx}(t) & \mathcal{G}_{yy}(t) & \mathcal{G}_{yz}(t) \\ \mathcal{G}_{zx}(t) & \mathcal{G}_{zy}(t) & \mathcal{G}_{zz}(t) \end{bmatrix}. \tag{8}$$

The integral is split into intervals of the length Δt. By calculating the mean of the upper and lower value, the soil displacements for the time step $i+1$ can be deduced

$$\mathbf{w}^{i+1} = \frac{\mathcal{G}^{i+1} - \mathcal{G}^{i}}{2}\cancelto{0}{\mathbf{q}^{0}} + \frac{\mathcal{G}^{i+1} - \mathcal{G}^{i-1}}{2}\mathbf{q}^{1} + \ldots + \frac{\mathcal{G}^{1} - \cancelto{0}{\mathcal{G}^{0}}}{2}\mathbf{q}^{i+1} \tag{9}$$

Subsequently, the flexibility of the soil is obtained after inserting the following abbreviations valid for constant time step duration for the whole simulation

$$\begin{aligned} \mathbf{F}^i &= \frac{1}{2}\left(\mathcal{G}^{i+1} - \mathcal{G}^{i-1}\right) \\ \mathbf{F}^{cur} &= \frac{1}{2}\mathcal{G}^1 = \frac{1}{2}\mathcal{G}(\Delta t) \end{aligned} \tag{10}$$

and considering the initial condition $\mathbf{q}^0 = 0$ and the relation $\mathcal{G}^0 = 0$, which results from causality, the deformations of the soil yield

$$\mathbf{w}^{i+1} = \underbrace{\mathbf{F}^i\mathbf{q}^1 + ... + \mathbf{F}^1\mathbf{q}^i}_{\mathbf{w}^{hist}} + \mathbf{F}^{cur}\mathbf{q}^{i+1} \tag{11}$$

If, additionally, a seismic excitation $\mathbf{s}$ occurs, one has to substitute the absolute displacements at the interaction nodes $\mathbf{w}^{i+1}$ with the relative displacements $(\mathbf{w}^{i+1} - \mathbf{s}^{i+1})$ to get

$$\mathbf{w}^{i+1} = \mathbf{w}^{hist} + \mathbf{F}^{cur}\mathbf{q}^{i+1} + \mathbf{s}^{i+1} \tag{12}$$

3 Implementation of the coupling

First, interaction nodes are defined, which are located at shared surfaces of the structure and the soil.

Fig. 2b shows the coupling surface between BEM and FEM for a square foundation. Since the numbering of the nodes is different for the BEM and the FEM subsytem, different letters identify different quantities:

- $\mathbf{u}_I$: displacements of the structure according to the nodal ordering of FEM at the interaction surface
- $\mathbf{v}$: displacements of the structure for nodal ordering of BEM at the interaction surface
- $\mathbf{w}$: displacements of the soil for nodal ordering of BEM at the interaction surface

The transformation matrices $\mathbf{T_u}$ and $\mathbf{T_q}$ help to couple the displacements of the two subsystems at the interface. These matrices are described in annex D.

From eq. (12), the soil's contact pressure can be computed as

$$\mathbf{q}^{i+1} = [\mathbf{F}^{cur}]^{-1}(\mathbf{w}^{i+1} - \mathbf{w}^{hist} - \mathbf{s}^{i+1}) \tag{13}$$

To satisfy compatibility at the interaction surface the structural displacements must equal the soil's displacement

$$\mathbf{w}^{i+1} = \mathbf{v}^{i+1} = \mathbf{T}_u\mathbf{u}_I^{i+1} \tag{14}$$

The soil reaction forces at the FEM nodes result from the combination of eq. (14) with eq. (15) as

$$\mathbf{Q}_I^{i+1} = \mathbf{T}_q\mathbf{q}^{i+1} = \underbrace{\mathbf{T}_q[\mathbf{F}^{cur}]^{-1}\mathbf{T}_u}_{\mathbf{K}_{soil}^{cur}}\mathbf{u}_I^{i+1} - \underbrace{\mathbf{T}_q[\mathbf{F}^{cur}]^{-1}\mathbf{w}^{hist}}_{\mathbf{Q}_I^{hist}} - \underbrace{\mathbf{T}_q[\mathbf{F}^{cur}]^{-1}\mathbf{s}^{i+1}}_{\mathbf{Q}_I^{seism}}, \tag{15}$$

where $\mathbf{K}_{soil}^{cur}$ is the soil's stiffness matrix.

Therefore, the equation of motion of the coupled problem becomes

$$\begin{bmatrix} \mathbf{M}_{RR} & \mathbf{M}_{RI} \\ \mathbf{M}_{IR} & \mathbf{M}_{II} \end{bmatrix} \begin{pmatrix} \ddot{\mathbf{u}}_R^{i+1} \\ \ddot{\mathbf{u}}_I^{i+1} \end{pmatrix} + \begin{bmatrix} \mathbf{C}_{RR} & \mathbf{C}_{RI} \\ \mathbf{C}_{IR} & \mathbf{C}_{II} \end{bmatrix} \begin{pmatrix} \dot{\mathbf{u}}_R^{i+1} \\ \dot{\mathbf{u}}_I^{i+1} \end{pmatrix} + \begin{bmatrix} \mathbf{K}_{RR} & \mathbf{K}_{RI} \\ \mathbf{K}_{IR} & \mathbf{K}_{II} + \mathbf{K}_{soil}^{cur} \end{bmatrix} \begin{pmatrix} \mathbf{u}_R^{i+1} \\ \mathbf{u}_I^{i+1} \end{pmatrix} = \begin{pmatrix} \mathbf{P}_R^{i+1} \\ \mathbf{P}_I^{i+1} \end{pmatrix} + \begin{pmatrix} 0 \\ \mathbf{Q}_I^{hist} + \mathbf{Q}_I^{seism} \end{pmatrix} \tag{16}$$

where I indicated the degrees of freedom (DOFs) at the interaction nodes, whereas the remaining DOFs are marked with R.

The flexibility matrix of the soil $\mathbf{F}^i$ in eq. (10) has to be calculated for every time step to deduce the quantity $\mathbf{w}^{hist}$.

The structural displacements $\mathbf{u}_I^i$ at the interaction nodes are computed by ANSYS at every time step and used to compute the soil reaction forces at $i+1$. The soil stiffness is added to the structure's stiffness through a user-defined super-element in ANSYS (element type *MATRIX50*) and the soil reactions are applied as external loads at the interaction nodes. The master DOFs of the soil super-element are the DOFs of the coupling nodes of the FEM-structure at the soil surface. With this configuration the system can be solved with usual solution routines in ANSYS. An overall calculation sequence for the proposed scheme is given in annex E.

It is to highlight, that, if the soil properties, the discretization of the elements at the interaction surface and the time step remain unchanged, a new analysis with different parameters and seismic and/or external loading can be carried out reusing the same flexibility matrix. This leads to a relevant reduction of computational time.

An interactive connection between MATLAB and ANSYS is created through the toolbox *aaS* (ANSYS as a Server) and the Mechanical APDL preprocessor and solver are accessed directly through MATLAB.

4 VERIFICATION

For the verification, we present the dynamic analysis of a rigid square foundation loaded with a Heaviside point load at its center. After the oscillation has decayed, the static displacement can be observed, so that also the static flexibility of the system can be compared to literature values. The results are compared to the ones found in [16], although we assume a Poisson's ratio $\nu = 0.25$ for the soil, while the reference results are computed with $\nu = 0.33$. As an additional reference, the static flexibility in different directions is compared to the reference values given in [22, p. 43].

As the results are normalized w.r.t. the quadratic foundation geometry and to the soil properties, the foundation side length a, the foundation thickness h, the shear modulus of the soil μ_s and the soil density ρ_s can be chosen arbitrarily. The Poisson's ratio is given ($\nu_s = 0.25$). The other problem parameters are given in tab. 1. In order to simplify the invetsigation, the Poisson's ratio of the foundation is set equal to 0, but could take any arbitrary value.

The vertical displacement u_z due to a vertical load P_z, the horizontal displacement u_x due to a horizontal load P_x, the rotation ϕ_y due to a moment around the y-axis M_y, the rotation ϕ_z due to a torsional moment M_z and finally the rotation ϕ_y due to a horizontal load P_x are examined. The loading starts at $\tau = \frac{tc_s}{a} = 1$. Two cases are investigated shown in fig. 4:

- massless foundation: the response follows the shape of the variation in time of the loading until it reaches a state of rest at $\approx \tau = 3$.

Table 1: Problem properties of the verification case.

Foundation density	massless foundation: $\rho_f = 0$
	massive foundation: $\rho_f = \frac{\rho_s}{h}\sqrt{\frac{a^2}{\pi}}$
Young's modulus of the foundation	$E_f \approx \mu_s * 10^{11}$
Poisson's ratio of the foundation	$\nu_f = 0$
Poisson's ratio of the soil	$\nu_s = 0.25$

- massive foundation: the foundation oscillated around the static response and, eventually, approaches the static solution at different times τ for the different directions of loading.

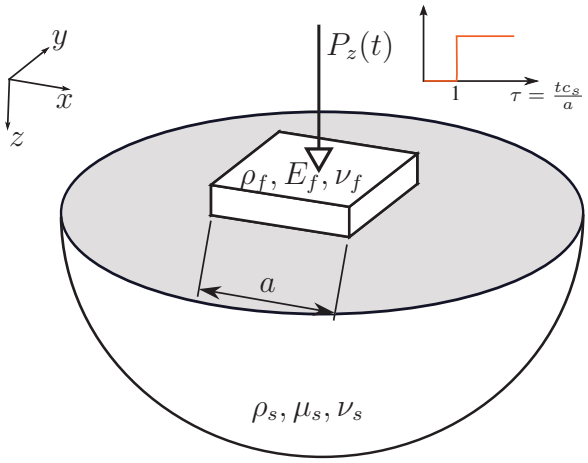

Figure 3: Verification case, shown for a vertical load.

The foundation and the soil surface are discretised with 8×8 elements with the side length $l = a/8$. The time step size is chosen as $\Delta t = 0.75l/c_s$, where $c_s = \sqrt{\frac{\mu_s}{\rho_s}}$ is the shear wave velocity of the soil.

The static flexibility is deduced from the displacements at rest. These are then compared in tab. 2 to the results from [16, pp. 107-111] and from the static stiffness values in [22, p. 43].

	$\frac{\mu_s a}{P_z}u_z$	$\frac{\mu_s a}{P_x}u_x$	$\frac{\mu_s a^3}{M_y}\phi_y$	$\frac{\mu_s a^3}{M_z}\phi_z$	$\frac{\mu_s a^2}{P_x}\phi_y$
Ssibefe	0.326	0.398	1.551	1.050	0.067
Bode [16]	0.2951	0.379	1.419	0.940	0.064
discrepancy [%]	1.11	1.05	1.09	1.12	1.05
Wolf [22]	0.319	0.380	1.5	0.964	-

Table 2: Static flexibility of a rigid, massless foundation on a homogeneous half-space.

As can be observed in tab. 2, the results are in good agreement. Nevertheless, small discrepancies especially between [16] and the results from *Ssibefe* occur for all modes, because of the different Poisson's ratios used. This is also confirmed in fig. 4a and fig. 4b, which show the transient displacements for the vertical and horizontal case respectively. Considering the different Poisson ratios, the different methods show a satisfying agreement.

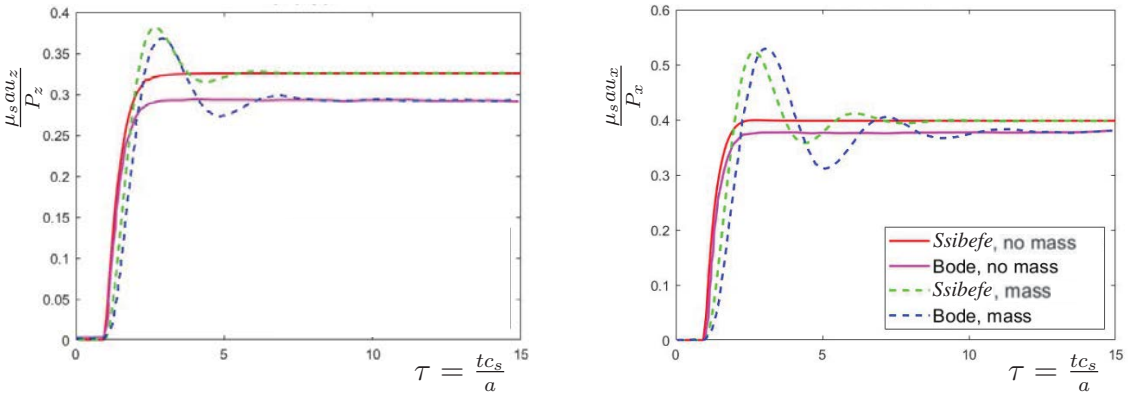

(a) Vertical displacement.

(b) Horizontal displacement.

Figure 4: Normalized displacements for a rigid square foundation subjected to a transient point load at the center in different directions.

5 SEISMIC APPLICATION OF THE *Ssibefe*

For the demonstration of the application of the *Ssibefe* for seismic problems, we present the dynamic analysis of an elastic cube of side length a resting on an elastic half space subjected to a seismic excitation resulting from an incident plane wave that propagates through the soil. Fig. 5 shows the investigated scenario.

Depending on the angle of incidence the wave, the direction of propagation and the time function, the seismic excitation at the interaction points $\mathbf{x}_I$ can be estimated according to eq. (17). The time function $s(t)$ of the plane wave can be chosen arbitrarily, from synthetic accelerogram to recorded data to analytical expressions. In this application, we assume a Ricker wavelet for the function $s(t)$, described by eq. (18) and plotted in fig. 6 for the specific loading parameters given in tab. 3.

$$\mathbf{s} = s\left(t - \frac{(\mathbf{x}_I - \mathbf{x}_0)^T \mathbf{n}}{c_{\text{ind}}}\right) \mathbf{s}_0 \tag{17}$$

$$s(t) = \left(1 - \pi^2 f_0^2 t^2\right) e^{\left(-\pi^2 f_0^2 t^2\right)} \tag{18}$$

The spectrum of the input is shown together with the output in fig. 9. In this application, the seismic wave propagates in the positive x-direction and the soil particles move along the x-axis, simulating a P-wave. The coordinates of the corner A of the building are $\mathbf{x} = [40\text{ m}, 5\text{ m}, 0\text{ m}]^T$ and the faces of the cubic building are oriented as the coordinate system.

The soil and structural properties are listed in tab. 5. The natural frequencies of the fixed-base cube are also given in tab. 4 for a better result interpretation. The element size is $l = 2.5$ m and the time step size is chosen equal to 0.025 s.

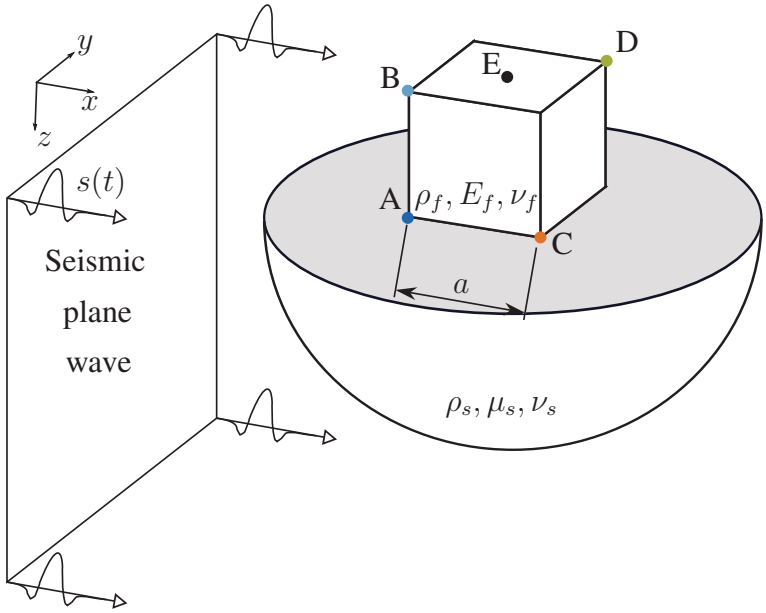

Figure 5: Building resting on an elastic half space subjected to a seismic excitation resulting from an incident plane wave that propagates through the soil.

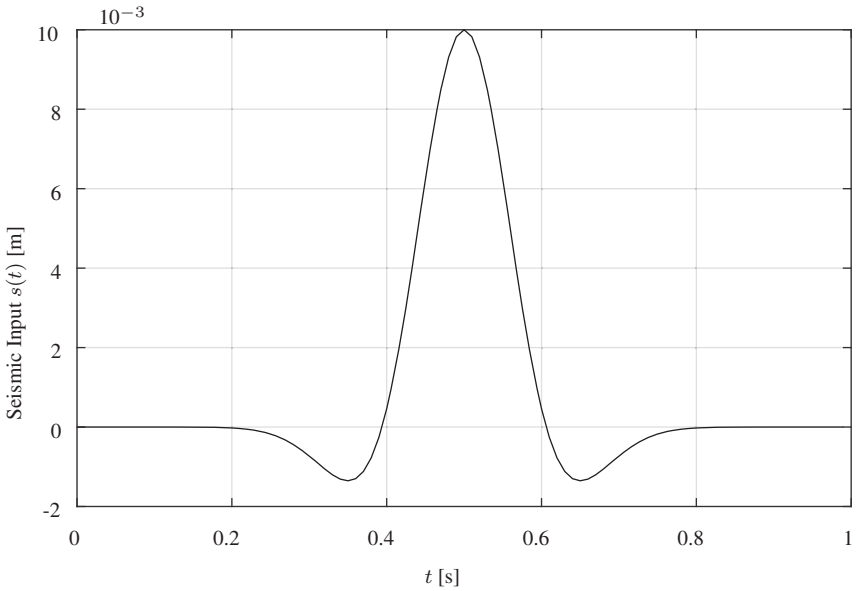

Figure 6: Time function of the seismic wave.

Table 3: Seismic load parameters.

Source position at $t = 0$	$\mathbf{x_0} = [0 \ 0 \ 0]^T$	[m]
Orientation of the wave	$\mathbf{n} = [1 \ 0 \ 0]^T$	[-]
Amplitude of the wave	$\mathbf{s}_0 = [0.01 \ 0 \ 0]^T$	[m]
Incident wave velocity	$c_{\text{ind}} = c_p = \sqrt{\frac{2\mu_s(1-\nu_s)}{1-2\nu_s}}$	[m/s]
Central frequency of the Ricker wavelet	$f_0 = 3$	[Hz]

Table 4: Soil and Structural properties.

μ_s	$40{\cdot}10^6$	[N/m^2]
ρ_s	2200	[Kg/m^3]
ν_s	0.25	[-]
a	40	[m]
E_f	$83{\cdot}10^6$	[N/m^2]
ρ_f	1000	[Kg/m^3]
ν_f	0.3	[-]

Table 5: Natural frequencies of the fixed-base building.

1. bending x, y	0.76750	[Hz]
1. torsion/bending	1.0436	[Hz]
1. axial	1.8322	[Hz]
2. bending x, y	2.0320	[Hz]
2. torsion/bending	2.5050	[Hz]
3. torsion/bending	3.0997	[Hz]
4. torsion/bending	3.1589	[Hz]
1. bending z	3.1680	[Hz]
2. axial/bending	3.5130	[Hz]

The results are compared to the ones obtained with the FEM/BEM coupling proposed by Bode [23], which runs on a ANSYS/FORTRAN Framework. The authors had the possibility to run the same identical example with both the existing framework [23] and the newly implemented *Ssibefe*. The only difference is the material damping in the soil, which we assumed equal to zero, while in Bode [23] it is small (0.1%) but not exactly zero. In the following discussion, only the horizontal displacements are shown, being those the largest. However, all the components of displacements and stresses can be computed.

Fig. 7 shows the horizontal displacements at the building base, at A and C. The delay of the wave arrival between the two points is correctly represented. Fig. 8 shows the horizontal displacements at the building top, at B and D and E. The spectra in fig. 9 show that the response at E is characterized by a natural frequency 0.6 Hz, which corresponds to the natural frequency of the 1st bending mode of the fixed-base building (0.76750 Hz) considering the influence of the soil. At the corners B and D also higher modes play an important role, as shown in fig. 9.

All the plots show good agreement between the reference results (Bode [23]) and the proposed results based on the *Ssibefe* tool. In general, there is a very slight difference of damping during the final oscillations, which leads to slightly different amplitudes and periods of oscillation. However, the difference can be neglected.

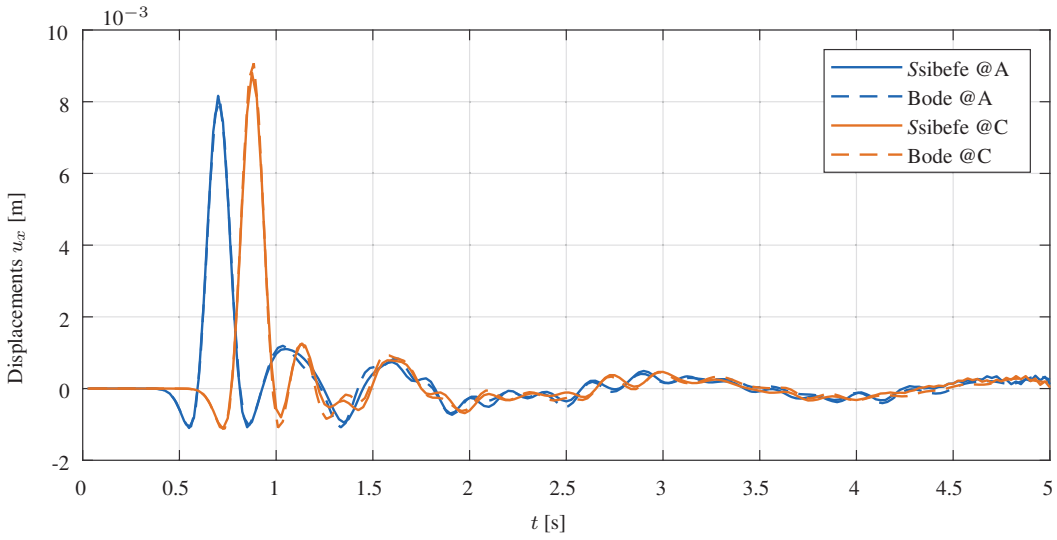

Figure 7: Horizontal displacements at the building base, at A and C.

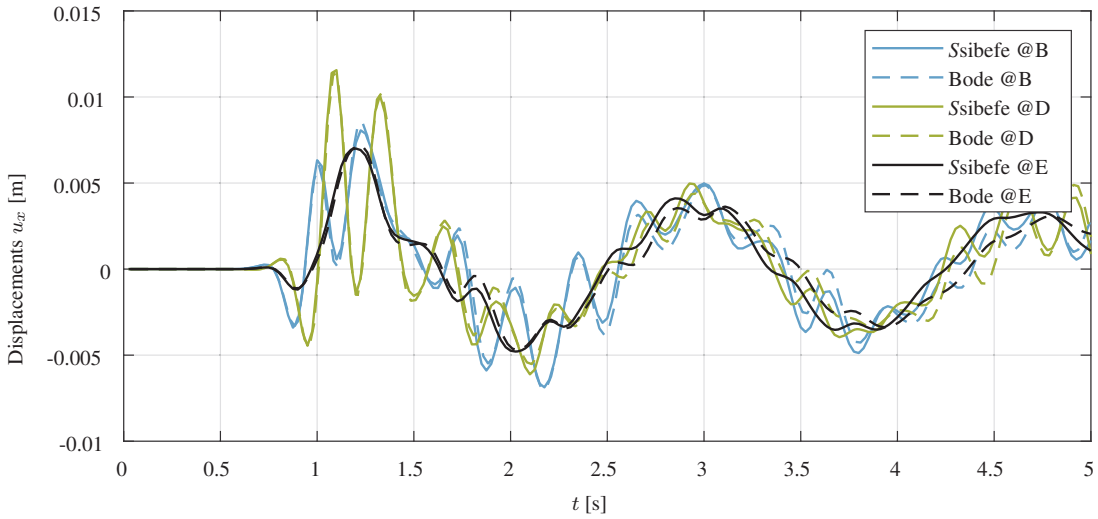

Figure 8: Horizontal displacements at the building top, at B and D and E.

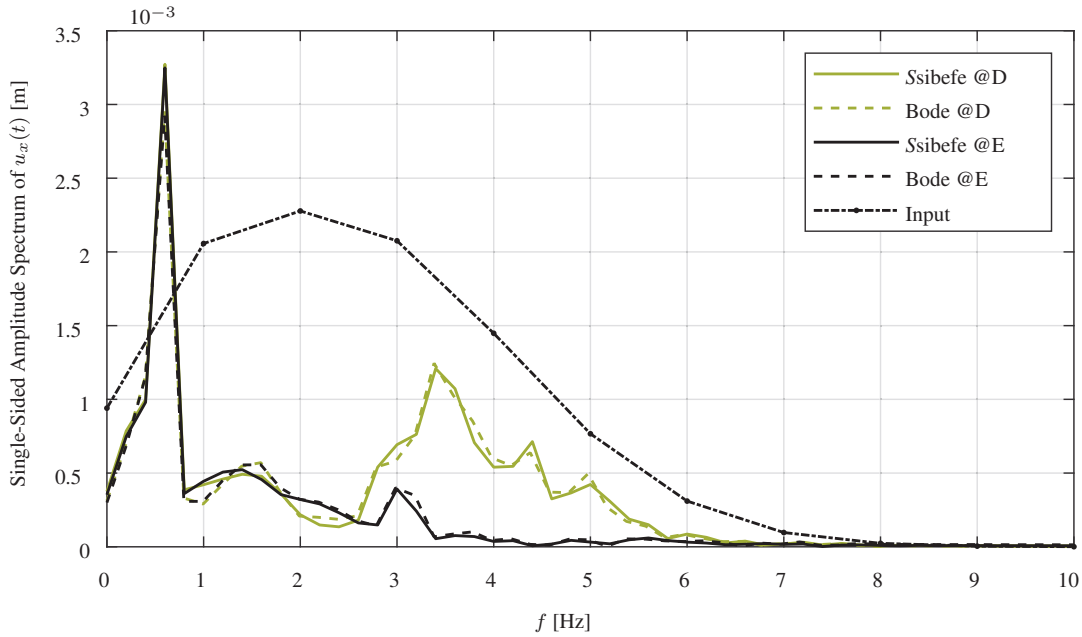

Figure 9: Spectra of the horizontal displacements at D and E, compared to the spectrum of the time function of the seismic wave.

6 CONCLUSIONS

In this contribution, we presented a new implementation of the coupling between the BEM and the FEM for soil-structure interaction problems, in the time domain. The developed computer tool *Ssibefe* is based on an interactive connection between MATLAB and ANSYS. The FEM part is generated through the ASNYS preprocessor, the soil reaction forces and the soil dynamic stiffness are computed with MATLAB functions based on the BEM formulation . The generated quantities are combined together into the coupled system of equations of the SSI system and the resulting system is solved with usual ASNYS solver routines. We presented the theoretical background of the methods and the time discretization approach. The tool can be used for both external loads on the structure and seimsic excitation. For the verification, we presented the dynamic analysis of a rigid square foundation loaded with a Heaviside point load at its center. The dynamic response as well as the static flexibility were compared to literature values, showing good agreement between the references and the results of the new implementation. Finally, we demonstrated the applicability of the *Ssibefe* tool for seismic problems, showing the dynamic analysis of an elastic cube of side length a resting on an elastic half space subjected to a seismic excitation resulting from an incident plane wave that propagates through the soil. The results match those from a reference software and show the potential of the proposed tool. Further developments of the *Ssibefe* tool will enable the consideration of layered soils, using fundamental solutions in the frequency domain, and additional forms of the seismic excitation.

REFERENCES

[1] N. Sharma, K. Dasgupta, and A. Dey, "A state-of-the-art review on seismic ssi studies on building structures," *Innovative Infrastructure Solutions*, vol. 3, no. 1, p. 22, 2018.

[2] P. Dineva, G. Manolis, and F. Wuttke, "Fundamental solutions in 3d elastodynamics for the bem: A review," *Engineering Analysis with Boundary Elements*, vol. 105, pp. 47–69, 2019.

[3] O. Zienkiewicz, D. Kelly, and P. Bettess, "The coupling of the finite element method and boundary solution procedures," *International journal for numerical methods in engineering*, vol. 11, no. 2, pp. 355–375, 1977.

[4] G. Beer, "Finite element, boundary element and coupled analysis of unbounded problems in elastostatics," *International Journal for Numerical Methods in Engineering*, vol. 19, no. 4, pp. 567–580, 1983.

[5] S. Ahmad and P. Banerjee, "Time-domain transient elastodynamic analysis of 3-d solids by bem," *International Journal for Numerical Methods in Engineering*, vol. 26, no. 8, pp. 1709–1728, 1988.

[6] D. Karabalis and D. Beskos, "Dynamic response of 3-d flexible foundations by time domain bem and fem," *International Journal of Soil Dynamics and Earthquake Engineering*, vol. 4, no. 2, pp. 91–101, 1985.

[7] C. Pekeris, "The seismic surface pulse," *Proceedings of the national academy of sciences of the United States of America*, vol. 41, no. 7, pp. 469–480, 1955.

[8] E. Kausel, *Fundamental Solutions in Elastodynamics: A Compendium*. Cambridge i.a.: Cambridge University Press, 2006.

[9] D. Rizos and D. Karabalis, "A time domain bem for 3-d elastodynamic analysis using the b-spline fundamental solutions," *Computational mechanics*, vol. 22, no. 1, pp. 108–115, 1998.

[10] D. Rizos, "A rigid surface boundary element for soil-structure interaction analysis in the direct time domain," *Computational Mechanics*, vol. 26, no. 6, pp. 582–591, 2000.

[11] I. Guzelbey, B. Kanber, and A. Erklig, "Coupling of finite and boundary element methods with incompatible interfaces," *Mathematical and Computational Applications*, vol. 10, no. 3, pp. 321–330, 2005.

[12] G. Vasilev, S. Parvanova, P. Dineva, and F. Wuttke, "Soil-structure interaction using bem-fem coupling through ansys software package," *Soil Dynamics and Earthquake Engineering*, vol. 70, pp. 104 – 117, 2015.

[13] P. Galvin and A. Romero, "A matlab toolbox for soil-structure interaction analysis with finite and boundary elements," *Soil Dynamics and Earthquake Engineering*, vol. 57, pp. 10 – 14, 2014.

[14] W. Schepers, "Fast 3d fem-bem coupling for dynamic soil-structure interaction," *Procedia engineering*, vol. 199, pp. 391–396, 2017.

[15] R. Hirschauer, *Kopplung von Finiten Elementen mit Rand-Elementen zur Berechnung der dynamischen Baugrund-Bauwerk-Interaktion*. PhD thesis, Technische Universität Berlin, 2001.

[16] C. Bode, *Numerisches Verfahren zur Berechnung von Baugrund-Bauwerk-Interaktionen im Zeitbereich mittels GREENnscher Funktionen für den Halbraum*. PhD thesis, Technische Universität Berlin, 2000.

[17] C. Bode, R. Hirschauer, and S. Savidis, "Soil–structure interaction in the time domain using halfspace green's functions," *Soil Dynamics and Earthquake Engineering*, vol. 22, no. 4, pp. 283–295, 2002.

[18] I. ANSYS, "Element reference," *ANSYS Mechanical APDL*, no. Release 15.0, 2013.

[19] A. Romero, D. López-Mendoza, and P. Galvin, "Bem-fem formulation in time domain for ssi analyses in layered soils," *Compdyn 2015*, 2015.

[20] G. Beer, I. Smith, and C. Duenser, *The boundary element method with programming: for engineers and scientists*. Wien: Springer Science & Business Media, 2010.

[21] L. Gaul, M. Kögl, and M. Wagner, *Boundary element methods for engineers and scientists: an introductory course with advanced topics*. Berlin i.a.: Springer Science & Business Media, 2003.

[22] J. Wolf, *Soil-structure-interaction analysis in time domain*. Englewood Cliffs: Prentice Hall, 1988.

[23] C. Bode, R. Hirschauer, and S. A. Savidis, "Soil-structure interaction in the time domain using halfspace green's functions," *Soil Dynamics and Earthquake Engineering*, vol. 22, no. 4, pp. 283 – 295, 2002.

Appendices

A Green's Functions

In this section the above mentioned fundamental solutions are shown [8, p.78-83].

A.1 Vertical load

$$r = \sqrt{x^2 + y^2} \quad \text{distance between loading and source point} \tag{A.1}$$

$$a^2 = \left(\frac{c_s}{c_p}\right)^2 = \frac{1-2\nu}{2(1-\nu)} \quad \text{ratio of s- and p-wave velocity} \tag{A.2}$$

$$\tau = \frac{t c_s}{r} \quad \text{dimensionless time} \tag{A.3}$$

$$H(t-t_0) = \left\{ \begin{array}{ll} 1 & t > t_0 \\ \frac{1}{2} & t = t_0 \\ 0 & t < t_0 \end{array} \right\} \text{Heaviside step function} \tag{A.4}$$

$$K(k) = \int_0^{\pi/2} \frac{d\theta}{\sqrt{1-k^2\sin(\theta)^2}} \quad \text{complete first elliptic integral} \tag{A.5}$$

$$\Pi(n,k) = \int_0^{\pi/2} \frac{d\theta}{(1+n\sin(\theta)^2)\sqrt{1-k^2\sin(\theta)^2}} \quad \text{complete third elliptic integral} \tag{A.6}$$

$$R(\xi^2) = (1-2\xi^2)^2 + 4\sqrt{\xi^2-1}\sqrt{\xi^2-a^2} = 0 \quad \text{Rayleigh function} \tag{A.7}$$

with $\xi = c_s/c$ a dimensionless wave slowness including the wave velocity c.

The Rayleigh function is further multiplied by $(1-2\xi^2)^2 + 4\sqrt{\xi^2-1}\sqrt{\xi^2-a^2}$ to obtain the bicubic equation

$$1 - 8\xi^2 + 8\xi^4(3-2a^2) - 16\xi^6(1-a^2) = 0 \tag{A.8}$$

For this equation the three roots $[\xi_1^2, \xi_2^2, \xi_3^2]$ are being calculated. The first two are non-physical values whereas $\xi_3 = c_s/c_r$ equals the ratio of shear and Rayleigh wave velocity. Due to considerations of real and complex roots of equation (A.8) the solutions of the half-space u_{zz} and u_{rz} are split into two domains ($\nu < 0.2631$ and $\nu > 0.2631$). Additionally, the numerical calculation of the first and third kind of the elliptic integral has to be implemented. This is done by adapting some parts but still applying the MATLAB code according to [8, pp. 250f.]. Further parameters are derived as follows

$$A_i = \frac{(1-2\xi_i^2)^2\sqrt{\|a^2-\xi_i^2\|}}{4(\xi_i^2-\xi_j^2)(\xi_i^2.-\xi_k^2)} \quad \xi_i \neq \xi_j \neq \xi_k \tag{A.9}$$

$$B_i = \frac{(1-2\xi_i^2)(1-\xi_i^2)}{(\xi_i^2-\xi_j^2)(\xi_i^2-\xi_k^2)} \quad \xi_i \neq \xi_j \neq \xi_k \tag{A.10}$$

$$k^2 = \frac{\tau^2 - a^2}{1-a^2} \tag{A.11}$$

$$n_i = \frac{1-a^2}{a^2-\xi_i^2} \tag{A.12}$$

$$C = \frac{(2\xi_3^2-1)^3}{1-4\xi_3^2+8(1-a^2)\xi_3^6} \tag{A.13}$$

$$Q_1(\tau) = 1 + 2z + \sqrt{z^2+z} \tag{A.14}$$

$$z = \frac{a^2-\xi_1^2}{\tau^2-a^2} \tag{A.15}$$

Important to notice is the fact that Q_1 should be replaced with $1/Q_1$ if $|Q_1| > 1$. With these definitions the displacements u_{zz} and u_{rz} can finally be obtained by

Case 1: $\nu < 0.2631$

$$u_{zz} = \frac{P(1-\nu)}{2\pi\mu r} \left\{ \begin{array}{ll} 0 & \tau < a \\ \frac{1}{2}\left[1 - \sum_{i=1}^3 \frac{A_i}{\sqrt{\|\tau^2-\xi_i^2|}}\right] & a < \tau < 1 \\ 1 - \frac{A_3}{\sqrt{\xi_3^2-\tau^2}} H(\xi_3 - \tau) & \tau > 1 \end{array} \right\} \tag{A.16}$$

$$u_{rz} = \frac{P\tau}{8\pi^2\mu r} \left\{ \begin{array}{ll} 0 & \tau < a \\ \frac{1}{(1-a^2)^{3/2}} \left[2K(k) - \sum_{i=1}^3 B_i \Pi(k^2 n_i, k)\right] & a < \tau < 1 \\ \frac{k^{-1}}{(1-a^2)^{3/2}} \left[2K(k^{-1}) - \sum_{i=1}^3 B_i \Pi(n_i, k^{-1})\right] + \frac{2\pi C}{\sqrt{\tau^2-\xi_3^2}} H(\tau - \xi_3) & \tau > 1 \end{array} \right\} \tag{A.17}$$

Case 2: $\nu > 0.2631$

u_{rz} not available

$$u_{zz} = \frac{P(1-\nu)}{16\pi\mu r} \left\{ \begin{array}{ll} 0 & \tau < a \\ 8Re\left[\frac{(1-2\xi_1^2)^2(a^2-\xi_1^2)}{(\xi_1^2-\xi_2^2)(\xi_1^2-\xi_3^2)} \frac{1}{Q_1 - Q_1^{-1})}\right] + \frac{A_3}{\sqrt{\xi_3^2-\tau^2}} - 4 & a < \tau < 1 \\ \frac{2A_3}{\sqrt{\xi_3^2-\tau^2}} H(\xi_3 - \tau) - 8 & \tau > 1 \end{array} \right\} \tag{A.18}$$

A.2 Horizontal load

For a horizontal load the quantities u_{rx} and $u_{\theta x}$ are only known in case of the Poisson's ratio $\nu = 0.25$. Again some parameters have to be defined.

$$a_h = \frac{1}{3}\sqrt{3}, \quad \xi_1^2 = \frac{1}{4}, \quad \xi_2^2 = \frac{1}{4}(3-\sqrt{3}), \quad \xi_3^2 = \frac{1}{4}(3+\sqrt{3}) \tag{A.19}$$

$$C_1 = \frac{3}{4}\sqrt{3}, \quad C_2 = \frac{1}{8}\sqrt{6\sqrt{3}+10}, \quad C_3 = \frac{1}{8}\sqrt{6\sqrt{3}-10} \tag{A.20}$$

Subsequently, the displacements can be calculated

$$u_{rx} = \frac{P}{2\pi\mu r}\left\{\begin{array}{ll} 0 & \tau < a_h \\ \tau^2\left[\frac{C_1}{\sqrt{\tau^2-\xi_1^2}} - \frac{C_2}{\sqrt{\tau^2-\xi_2^2}} - \frac{C_3}{\sqrt{\xi_3^2-\tau^2}}\right] & a_h < \tau < 1 \\ 1 - \frac{2\tau^2 C_3}{\sqrt{xi_3^2-\tau^2}}[1-H(\tau-\xi_3)] & \tau > 1 \end{array}\right\} \tag{A.21}$$

$$u_{\theta x} = \frac{-3P}{8\pi\mu r}\left\{\begin{array}{ll} 0 & \tau < a_h \\ \left[\frac{1}{2} - \frac{4}{3}(C_1\sqrt{\tau^2-\xi_1^2} - C_2\sqrt{\tau^2-\xi_2^2} + C_3\sqrt{\xi_3^2-\tau^2})\right] & a_h < \tau < 1 \\ 1 - \frac{8}{3}C_3\sqrt{\xi_3^2-\tau^2}[1-H(\tau-\xi_3)] & \tau > 1 \end{array}\right\} \tag{A.22}$$

The above derived relations for the displacements due to horizontal and vertical loads are plotted while being scaled with the shear modulus μ and the distance r in the figures A.1 to A.4. For the later description via the tensor $\mathbf{g}$ according to [15], the quantities are written in a new notation, acconting for a changed coordinate system (the z-axis in the *Ssibefe* tool points downward while it was defined upward in [8]).

$$g_{zz} = u_{zz}, \quad g_{rz} = -u_{rz}, \quad g_{rr} = u_{rx}, \quad g_{\phi\phi} = -u_{\theta x}, \quad g_{zr} = u_{rz} \tag{A.23}$$

B Coordinate Transformation

The coordinate transformation

$$\mathbf{g}^{cart} = \mathbf{B}^T(\phi)\mathbf{g}^{cyl}\mathbf{B}(\phi) \tag{B.24}$$

can be accomplished by the rotation matrix

$$\mathbf{B}(\phi) = \begin{bmatrix} \cos(\phi) & \sin(\phi) & 0 \\ -\sin(\phi) & \cos(\phi) & 0 \\ 0 & 0 & 1 \end{bmatrix} \tag{B.25}$$

This leads to tab. B.1.

$g_{xx} = g_{rr}\cos^2(\phi) + g_{\phi\phi}\sin^2(\phi)$	$g_{xy} = (g_{rr} - g_{\phi\phi})\cos(\phi)\sin(\phi)$	$g_{xz} = g_{rz}\cos(\phi)$
$g_{yx} = g_{xy}$	$g_{yy} = g_{rr}\sin^2(\phi) + g_{\phi\phi}\cos^2(\phi)$	$g_{yz} = g_{rz}\sin(\phi)$
$g_{zx} = g_{zr}\cos(\phi) = -g_{xz}$	$g_{zy} = g_{zr}\sin(\phi) = -g_{yz}$	$g_{zz} = g_{zz}$

Table B.1: Green's functions in Cartesian coordinates.

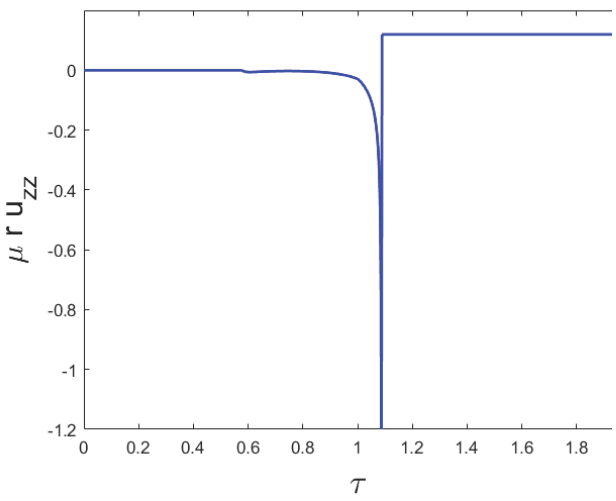

Figure A.1: Vertical displacement due to vertical load, $\nu = 0.25$.

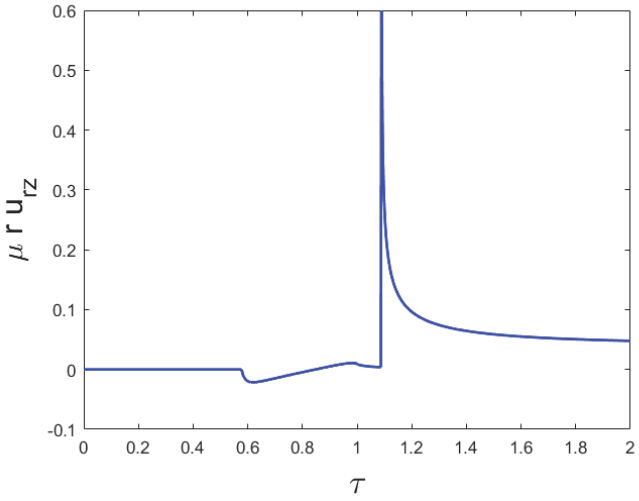

Figure A.2: Radial displacement due to vertical load, $\nu = 0.25$.

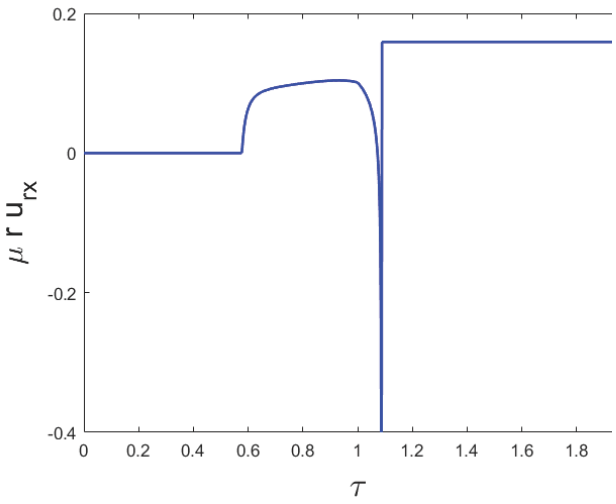

Figure A.3: Radial displacement due to horizontal load, $\nu = 0.25$.

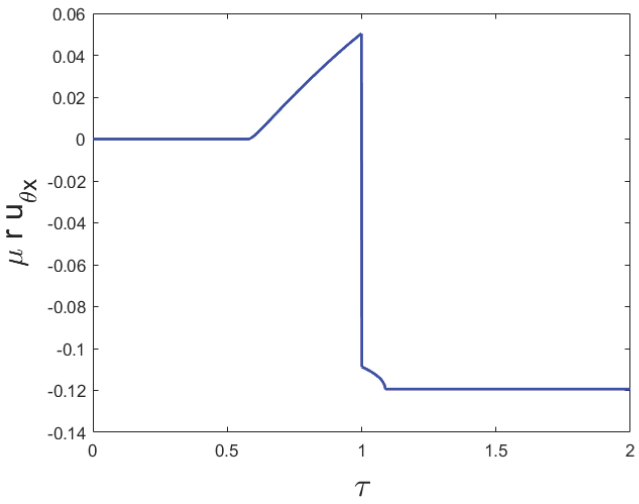

Figure A.4: Tangential displacement due to horizontal load, $\nu = 0.25$.

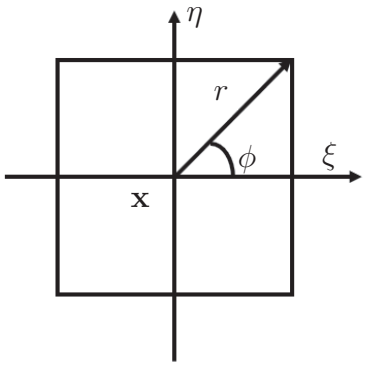

Figure C.1: Transformation to polar coordinates for constant boundary elements.

C Transformation to polar coordinates

To regularise the weak singularity of the integrand in eq. (4) a transformation to polar coordinates according to [21] can be used.

$$\Delta \mathbf{G}_n^e = \sum_{m=1}^{M} \sum_{k=1}^{K} \mathbf{N}_n(\xi_m, \eta_k) \mathbf{g}(r(\xi_m, \eta_k), \phi(\xi_m, \eta_k), t) J(\xi_m, \eta_k) W_m W_k \tag{C.1}$$

The coordinate system for constant elements is located in the centre of the element because the origin of the coordinate system should be at the loading node (see fig. C.1). The radius and the angle are adapted as follows

$$r(\xi, \eta) = \sqrt{\xi^2 + \eta^2} \qquad \phi(\xi, \eta) = atan2\left(\frac{\eta}{\xi}\right) \tag{C.2}$$

For the calculation of the Jacobian determinant changes of the partial derivatives occur

$$\begin{aligned} \frac{\partial r}{\partial \xi} &= \frac{\xi}{\sqrt{\xi^2 + \eta^2}} & \frac{\partial \phi}{\partial \xi} &= -\frac{\eta}{\xi^2 + \eta^2} \\ \frac{\partial r}{\partial \eta} &= \frac{\eta}{\sqrt{\xi^2 + \eta^2}} & \frac{\partial \phi}{\partial \eta} &= \frac{\xi}{\xi^2 + \eta^2} \end{aligned} \tag{C.3}$$

Except for these adaptations, formula (C.1) is valid for the constant elements as well. Since this regularisation approach led to the best results, it is used for all further calculations in this thesis.

D Transformation matrices from BEM to FEM

$$\mathbf{T}_u = \begin{bmatrix} [\mathbf{N}] & [\mathbf{0}] & [\mathbf{0}] \\ [\mathbf{0}] & [\mathbf{N}] & [\mathbf{0}] \\ [\mathbf{0}] & [\mathbf{0}] & [\mathbf{N}] \end{bmatrix} \tag{D.1}$$

with e.g.

$$\mathbf{N} = \begin{bmatrix} N_M & 0 & 0 & 0 & \dots \\ 0 & 0 & N_P & 0 & \dots \\ \dots & \dots & \dots & \dots & \dots \end{bmatrix} \tag{D.2}$$

$$\mathbf{T}_q = \mathbf{T}_u^T \mathbf{A} \tag{D.3}$$

with the matrix $\mathbf{A}$ which contains the element area as a diagonal matrix.

E Workflow of the *Ssibefe* tool

Figure E.1: Workflow of the *Ssibefe* tool.